Acta Biomaterialia 189 (2024) 366–376

Contents lists available at ScienceDirect

Acta Biomaterialia

journal homepage: www.elsevier.com/locate/actbio

Full length article

Stress relaxation behavior of the transition zone in the intervertebral disc

Lydia Vieira[a,1], Haim S Mordechai[b,1], Mirit Sharabi[b,*], Joanne L. Tipper[a,c,**], Javad Tavakoli[a,c,**]

[a] School of Biomedical Engineering, Faculty of Engineering and Information Technology, University of Technology Sydney, NSW 2007, Australia
[b] Department of Mechanical Engineering and Mechatronics, Ariel University, Ariel 407000, Israel
[c] Department of Biomedical Engineering, School of Engineering, RMIT University, VIC 3000, Australia

ARTICLE INFO

Article history:
Received 12 June 2024
Revised 8 September 2024
Accepted 18 September 2024
Available online 24 September 2024

Keywords:
Intervertebral disc
Transition zone
Stress relaxation
Nucleus pulposus
Annulus fibrosus
Modelling

ABSTRACT

The stress relaxation of the TZ region, located at the interface of the Annulus Fibrosus (AF) and Nucleus Pulposus (NP) of the disc, and how its stress is relaxed compared to the adjacent regions is unknown. The current study aimed to identify the TZ stress relaxation properties under different strain magnitudes (0.2, 0.4, and 0.6 mm/mm) and compared the TZ stress relaxation characteristics to the NP and inner AF (IAF) regions at a specific strain magnitude (0.6 mm/mm). The results of the current study revealed that the TZ region exhibited different stress relaxation properties under various strain magnitudes with significantly higher initial ($p < 0.008$) and reduced stresses (marginally; $p = 0.06$) at higher strains. Our experimental stress relaxation data revealed a significantly higher equilibrium stress for the IAF compared to the TZ and NP regions ($p < 0.001$) but not between the TZ and NP regions ($p = 0.7$). We found that NP radial stress relaxed significantly faster ($p < 0.04$) than the TZ and NP. Additionally, the current study proposed a simple mathematical model and identified that, consistent with experimental data, the overall effect of region on both the level of decayed stress and the rate at which stress is relaxed was significant ($p < 0.006$). The current study found a similar stress relaxation characteristic between the NP and TZ regions, while IAF exhibited different stress relaxation properties. It is possible that this mismatch in stress relaxation acts as a shape transformation mechanism triggered by viscoelastic behavior.

Statement of significance

Our understanding of the biomechanical properties of the transition zone (TZ) in the IVD, a region at the interface of the Nucleus Pulposus (NP) and Annulus Fibrosus (AF), is sparse. Unfortunately, there are no current studies that investigate the TZ stress relaxation properties and how stress is relaxed in the TZ compared to the adjacent regions. For the first time, the current study characterized the stress relaxation properties of the TZ and described how the TZ stress is relaxed compared to its adjacent regions.

1. Introduction

The intervertebral disc (IVD), a complex and dynamic structure that is located between adjacent vertebrae in the spine, is comprised of two main regions: the Annulus Fibrosus (AF) and the Nucleus Pulposus (NP). The AF is a concentric and multilayered structure surrounding the NP, a gelatinous structure situated centrally within the IVD [1]. The AF-NP interface, known as the Transition Zone (TZ), has been the subject of very few studies; hence, our understanding of its biomechanical and structural role has yet to be determined. It is believed that the TZ region mediates the transfer of mechanical loads, allowing for the essential interplay of mechanical and biological functions [2–4]. Biological studies have shown that TZ facilitates nutrient transport, maintains a balance between structural stability and flexibility, and controls the exchange of metabolites [5–7]. Using animal models such as rabbit

* Corresponding author.
** Corresponding authors at: School of Biomedical Engineering, Faculty of Engineering and Information Technology, University of Technology Sydney, NSW 2007, Australia.
E-mail addresses: miritsh@ariel.ac.il (M. Sharabi), joanne.tipper@rmit.edu.au (J.L. Tipper), javad.tavakoli@rmit.edu.au (J. Tavakoli).
[1] Equal first authorship contribution.

https://doi.org/10.1016/j.actbio.2024.09.032
1742-7061/

and porcine, higher metabolic activity and stiffer cells (≈ 3 times) were observed in the TZ compared to the NP region, indicating the impact of the structural hierarchy of the TZ on cell and extracellular matrix properties [6–8].

Recent studies have focused on the TZ structural organization at the fiber level and its biomechanical properties [9–11]. These studies revealed that parallel elastic fibers in the NP running towards the AF merged to form an elastic network at the TZ region [11]. The TZ elastic network is subsequently integrated into the AF fibers via adaptation, direct penetration, and entanglement mechanisms [9]. Further investigations into the biomechanical properties of the TZ region under different loading scenarios (non-physiological and physiological loading) clarified the critical role of the TZ in the adjustment of the stiffness gradient which increases from the NP towards the AF [9,10]. While these studies have enhanced our understanding of the contribution of the TZ region to the overall IVD structural integrity and its biomechanical properties, how stress is relaxed at the AF-NP interface is yet to be explored. Stress relaxation involves complex interactions between IVD fluid flow, viscoelasticity, and fiber organization [12–14]. The redistribution of IVD fluid, realignment of fibers, and gradual deformation of tissue in response to sustained mechanical loading contribute to the dissipation of stress over time and influence the biomechanical characteristics of the IVD. Therefore, abnormal stress relaxation behavior can be a sign of IVD structural deficiencies leading to stress relaxation-associated pathologies [15,16]. Insights into the TZ stress relaxation characteristics, including excessive or abnormal stress relaxation, can enhance our knowledge of the TZ potential contribution to chronic low back pain development.

Several studies have investigated the time-dependent deformation, including stress relaxation properties, of IVD as a whole and have used different mathematical approaches such as linear and non-linear viscoelastic modelling to identify the impact of hydration and osmotic properties, structure, degeneration grade, low-frequency vibration, and loading cycles on the overall IVD viscoelastic and stress relaxation properties [12,17–26]. These investigations have shown that the IVD response to cyclic loading exhibits a nonlinear plateauing effect with reduced relaxation, which can be fully restored after unloading [24,27]. Additionally, it was explained that swelling (due to osmosis) and fiber-induced equilibrium strain (due to structural complexity) are important parameters for developing a more physiological model to predict AF stress relaxation behavior [28]. It was also found that injured IVDs exhibited significantly less stress relaxation, but using Fibgen hydrogel to repair the injury could noticeably improve their relaxation characteristics [29]. IVD relaxation, captured by MRI images, has been used to validate a numerical model for predicting mechanical response in uniaxial time-dependent compressive tests and the redistribution of tissue porosity after loading. The findings suggest that combining MRI imaging with finite element models enables the assessment of degenerative changes in IVDs [30]. While these studies have enhanced our understanding of the stress relaxation characteristics of the IVD, there are no current studies on the stress relaxation properties of the TZ region. Lack of knowledge of the TZ stress relaxation properties has motivated the authors to explore how stress is relaxed in this region, followed by exposure to different strain magnitudes in the radial direction (aim 1). Additionally, we compared the stress relaxation behavior in the radial direction of the TZ to the NP and inner AF regions for a specific strain magnitude (aim 2).

2. Materials and methods

Sample preparation in the current study included two stages. First, an IVD tissue was transversely cut to a thickness of 1 mm (from the middle of the IVD) using a custom-made double-blade device with trimming blades positioned 1 mm apart. Then, AF-TZ-NP tissue blocks, each measuring 5 mm in width and 30 mm in length, were dissected from the IVD tissue. A custom-made double-blade device with trimming blades positioned 5 mm apart was used for tissue block preparation (Fig. 1). The second stage was to select a 1 mm length of tissue from the inner annulus fibrosus (IAF), TZ, and NP regions of the tissue blocks using a tissue-labelling device. This device had two rectangles (L = 10 mm × W = 5 mm) with a 1 mm distance between them, highlighting the regions of interest. In the current study, the NP and TZ regions were defined as being 10 and 1 mm from the last layer of the AF, respectively. The IAF region was defined as being 3 mm from the last AF layer (towards the outer AF) (Fig. 1a). These regions were visually identified under microscope observation ensuring the consistency of the samples' dimensions (thickness, length, and width) as well as the selection of regions of interest across all samples for mechanical testing.

2.1. Sample preparation

Fresh frozen ovine spines (N = 38; > 18 months old) were obtained from a local abattoir and L4/5 functional spinal units (FSUs; IVDs with top and bottom vertebrae) were separated from the spines. FSUs were randomly organized into 5 groups (N = 6 each) for mechanical testing and another 2 groups (N = 4 each) for swelling characterization. While frozen, the top vertebra was carefully separated from each FSU, and the bottom vertebra was used to hold the sample to transversely cut an IVD tissue (1 mm thick) from the middle of each IVD. As explained in our previously published study, a custom-made double-blade cutting device, with the trimming blades 1 mm apart, was used to prepare IVD tissues [9]. Finally, tissue blocks (AF – TZ – NP) with 5 mm width and 30 mm length were dissected from the anterior region of the IVD tissues (Fig. 1a).

2.2. Sample preparation for mechanical testing

Samples for mechanical testing were prepared using a similar methodology determined in our previous works to measure the mechanical properties of the interlamellar matrix in the AF and the TZ region of the IVD [9,10,31,32]. Briefly, using a laser cutter (Fusion M2), two rectangles (L = 10 mm × W = 5 mm) with a 1 mm distance apart were cut from Kodak photo paper to prepare a tissue-labelling device. Moving the device over the surface of the IVD tissue block, under microscope observation (RL-M3T stereo microscope), allowed the identification of 1 mm × 5 mm (length × width) tissue from all regions of interest (inner AF; IAF, TZ, and NP) using a marker. Using cyanoacrylate adhesive, waterproof sandpapers were attached to the edge of the marked regions. In total, 30 samples (L = 1 mm × W = 5 mm × t = 1 mm), including 18 TZ samples (3 groups × 6 samples), 6 IAF samples (1 group × 6 samples), and 6 NP samples (1 group × 6 samples), were prepared to perform mechanical tests for the TZ, IAF, and NP regions, respectively (Fig. 1b).

2.3. Mechanical testing

An Electroforce testing machine (Biodynamic 5100, load cell capacity = 22 N, 0.2 % full-scale accuracy, TA Instruments, USA) was used to perform stress relaxation tests. To understand the stress relaxation behavior of the TZ region (the first aim of the study), separate TZ samples were stretched (ramp displacement with ramp time < 0.4 s) to 20 %, 40 %, and 60 % of their initial length (1 mm, equivalent to 0.2, 0.4, and 0.6 mm/mm, respectively) and were held

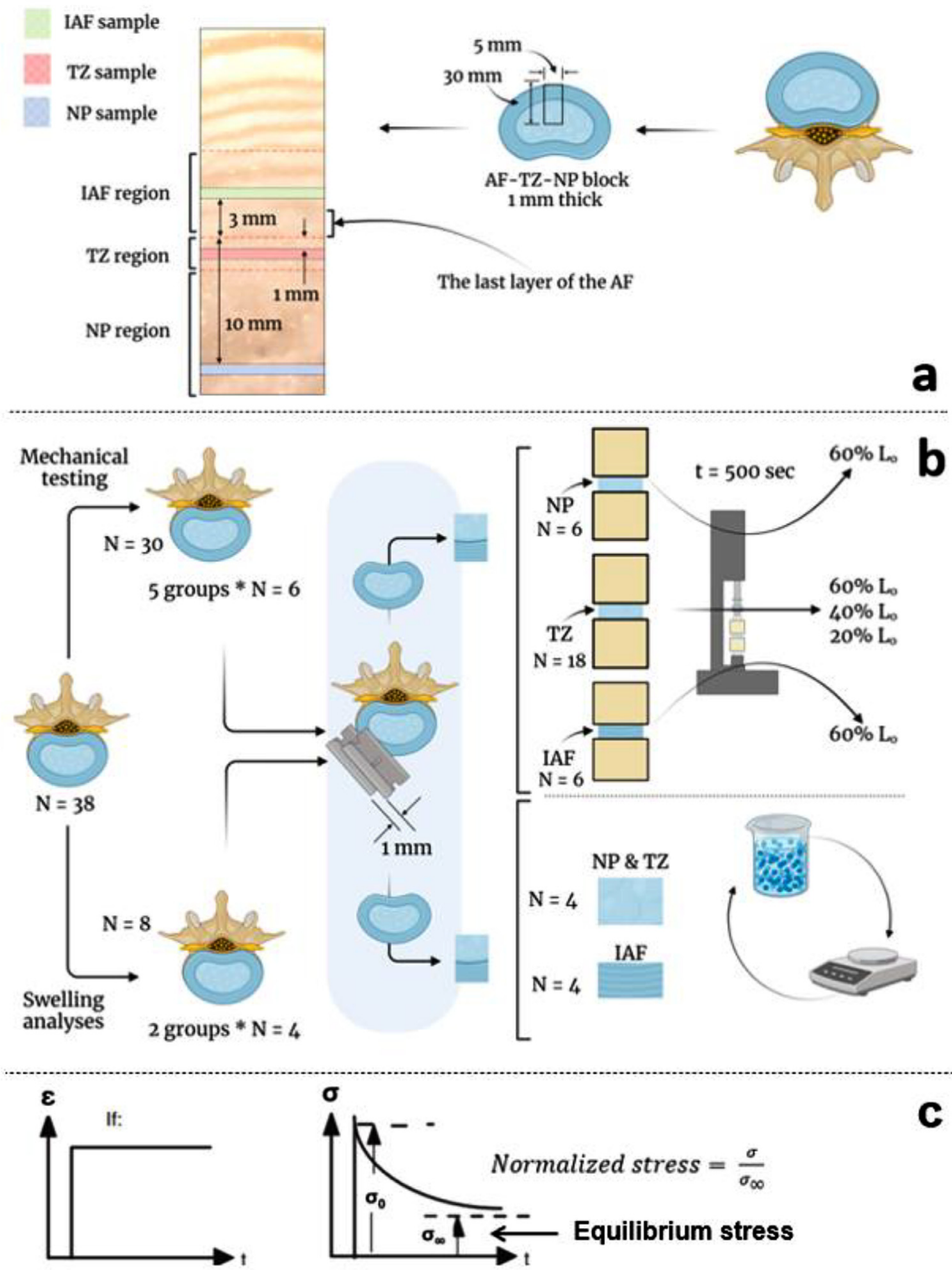

Fig. 1. a) The schematic diagram for the preparation of AF-TZ-NP tissue blocks from the anterior region of IVD, including the identification of the regions of interest for mechanical testing using microscopy of the tissue block (10X magnification). Fresh frozen ovine IVD tissues were transversely cut (thickness = 1 mm) from the middle of the IVD and AF-TZ-NP tissue blocks (5 mm in width × 30 mm in length) were dissected from the IVD tissue. A region of 1 mm in length was marked from the tissue blocks to highlight the IAF, TZ, and NP regions. The NP and TZ regions were defined as being 10 and 1 mm from the last layer of the AF, respectively. The IAF region was defined as being 3 mm from the last AF layer. b) The schematic diagram for sample preparation (mechanical testing and swelling characterization). Samples for mechanical testing were prepared using cyanoacrylate adhesive to attach waterproof sandpapers to the edge of the marked regions. In total, 30 samples (L = 1 mm × W = 5 mm × t = 1 mm), including 18 TZ samples (3 groups × 6 samples), 6 IAF and NP samples (1 group × 6 samples each) were prepared to perform mechanical tests. Samples were stretched at different strain magnitudes and were held for 500 s and changes in load as a function of time were then measured to calculate the stress relaxation over time. Another 8 samples were prepared to measure the swelling properties using a gravimetric method. c) Schematic for stress relaxation test and calculation of normalized stress.

for 500 sec. Changes in load as a function of time were then measured to ultimately calculate the stress relaxation over time. For the second aim of the study, to compare stress relaxation parameters between the TZ and adjacent regions, samples from the TZ, NP, and IAF were stretched to 0.6 mm/mm of their initial length, and relevant stress relaxations were measured over 500 sec (Fig. 1b). In our previously published studies, we found that structural failure of the AF tissue in the IVD initiates at 60–70 % radial stretch and delamination of the AF layers may occur. Therefore, in this study, we chose 0.6 mm/mm stretch to compare how stress is relaxed in the TZ (compared to the AF and NP regions) when the risk of failure in the AF is high [33,34]. All mechanical tests were performed in the radial direction under the application of 25 mN preload. Additionally, all samples were pre-soaked in water for different durations depending on the region (see swelling characterization) before the execution of mechanical testing. A humidity chamber was also used to maintain tissue hydration over time, which was connected to a portable tabletop compressor nebulizer (CareMax) creating a closed-loop circuit to supply water vapor during mechanical testing.

2.4. Sample preparation for swelling characterization

The sample preparation process for mechanical testing took approximately 20 min to prepare one sample. To understand the impact of the duration of sample preparation on their swelling characteristics, and consequently, develop a methodology to maintain tissue hydration before and during mechanical testing, IVD tissues were dissected from the NP-TZ and IAF regions (4 samples in each group). Since the TZ region in the IVD is a small region with less than 5 mm of length [11], it was almost impossible to measure the swelling properties of the TZ region alone accurately. Therefore, NP-TZ tissue blocks were selected to identify the associated swelling characteristics. Samples were initially placed at room temperature for 20 min (same conditions as for sample preparation), and water loss was measured gravimetrically. Then, samples were placed in a water bath, and their swelling ratio was determined until the samples reached the initial level of water content. Additionally, samples were placed in the humidity chamber for 500 s, and their water loss was determined as a function of time. The associated swelling properties for all samples were characterized gravimetrically using the following equation:

$$Water\ uptake\ \left[loss\right] = \frac{m_t - m_0}{m_0} \tag{1}$$

Where m_t and m_0 were the weights of samples at time t and 0, respectively.

2.5. Mechanical data

Stress relaxation characteristics of IVD samples were calculated based on changes in engineering stress as a function of time. Normalized stress was calculated as the ratio of stress and equilibrium stress (Fig. 1c). Stress relaxation parameters were calculated using a mathematical model presented by Peleg [35]:

$$Y(t) = \frac{abt}{1 + bt} \tag{2}$$

Where *Y(t)* and t represent stress decay and time, respectively, and a and b are constant stress relaxation parameters. *Y(t)* can be calculated using the following equation:

$$Y(t) = \frac{\sigma_0 - \sigma_t}{\sigma_0} \tag{3}$$

Where σ_0 and σ_t are the stresses calculated at time 0 and after t sec at relaxation, respectively.

One of the mathematical characteristics of Eq. (2) is that it gives a straight line when plotted in the form of the following equation:

$$\frac{1}{Y(t)} = \frac{1}{ab} + \frac{t}{a} \tag{4}$$

Using the Plege model, curves for both different regions and strain magnitudes were fitted to the experimental data, and the goodness of fit was assessed by calculating the coefficient of determination (R^2) values.

Constant parameter “a” refers to the level of stress that is decayed during relaxation, and parameter “b” represents the rate at which the tissue stress is relaxed. If a = 0, the stress is unlikely to relax (behavior of an ideal elastic solid), and the tissue stress level eventually reaches zero (i.e. liquids) if a = 1. For 0 < a <1, the tissue equilibrium stress has a value of Y. In general, the lower the stress relaxation, the lower the value of parameter b, and a higher b value indicates a sharper relaxation descent towards the equilibrium value.

2.6. Statistical analysis

For statistical analysis, separate One-Way ANOVAs (SPSS Statistics for Windows, Version 27.0. Armonk, NY: IBM Corp.) were performed, having test variables of stress decay level and relaxation rate for each of the regions of interest (AF, TZ, and NP; strain magnitude = 0.6 mm/mm of initial sample length) and the TZ region at different strain magnitude of 0.2, 0.4, and 0.6 mm/mm (alpha = 0.05). Post-hoc multiple comparisons using a Bonferroni adjustment on alpha were also performed to detect significant differences between samples.

3. Results

To maintain tissue hydration before and during mechanical testing, swelling analyses were performed for both TZ-NP and IAF samples separately to minimize the impact of IVD sample hydration levels on stress relaxation data. During sample preparation (20 min), both the IAF and NP-TZ samples became dehydrated with the water loss of the NP-TZ samples (20.5 ± 3.5 %) being significantly higher compared to the IAF sample (3.2 ± 0.3 %). Our swelling data revealed that the swelling ratio for both the IAF and NP-TZ samples reached the initial level (same level before the start of sample preparation) after 23 and 6 min, respectively (Fig. 2a). This was employed as a swelling protocol to prepare samples for mechanical testing. Hence, the IAF samples were soaked in water for 23 min before being placed in the humidity chamber before the execution of mechanical testing. Both TZ and NP samples were pre-soaked for 6 min in water prior to mechanical testing. To understand whether samples dehydrated during the stress relaxation test, they were placed in the humidity chamber for 500 s, and their water loss was measured gravimetrically at different time points. It was observed that water loss was negligible (< 2 %) for all samples from different regions of interest during mechanical testing (500 s) when a humidity chamber was used. The water loss from the NP -TZ as well as the AF samples during stress relaxation tests, were 1.7 ± 0.6 % and 1 ± 0.2 %, respectively (Fig. 2b).

Fig. 3a and b show the mean (± 95 % CI) stress relaxation curves for the TZ region at different strain magnitudes of 0.2, 0.4, and 0.6 mm/mm and for different regions of interest (IAF, TZ, and NP) at 0.6 mm/mm strain, respectively. The initial tissue stress was higher for higher strain magnitudes with an increasing trend from 0.2 to 0.6 mm/mm. Our normalized data for stress (to the equilibrium stress) revealed that the IAF exhibited a different stress relaxation behavior compared to the NP and TZ regions (Fig. 3c). While stress decay was approximately similar for both the TZ and NP regions, we observed a lower normalized stress for the IAF region. The observed mismatch in decay patterns for different IVD regions may affect the load transfer.

Our statistical analysis revealed that the initial TZ stress was significantly higher for 0.6 mm/mm strain (122.5 ± 17.4 kPa) compared to 0.4 mm/mm (74.6 ± 18.9 kPa; $p = 0.01$) and 0.2 mm/mm (40.7 ± 8.7 kPa; $p < 0.001$) strains. A higher initial TZ stress was also observed for 0.4 mm/mm compared to 0.2 mm/mm strain (marginally significant; $p = 0.06$) (Fig. 4a). For all strain magnitudes, the final average TZ stress was not decayed to zero with the mean (± 95 % CI) equilibrium stresses being 14.6 ± 5.3, 9.9 ± 3.1, and 6.1 ± 2.4 kPa for strain magnitudes of 0.6, 0.4, and 0.2 mm/mm, respectively. The TZ equilibrium stress was marginally different for different strain magnitudes ($p = 0.05$) (Fig. 4b).

The overall effect of the region (IAF, TZ, and NP) was significant for both initial and equilibrium stresses ($p < 0.001$) when samples were exposed to 0.6 mm/mm strain. The initial stress was significantly higher for the IAF (431.4 ± 27.8 kPa) compared to the TZ (122.5 ± 17.4 kPa; $p < 0.001$) and NP (34.7 ± 3.9 kPa; $p < 0.001$) regions (Fig. 4c). Additionally, the initial TZ stress was significantly

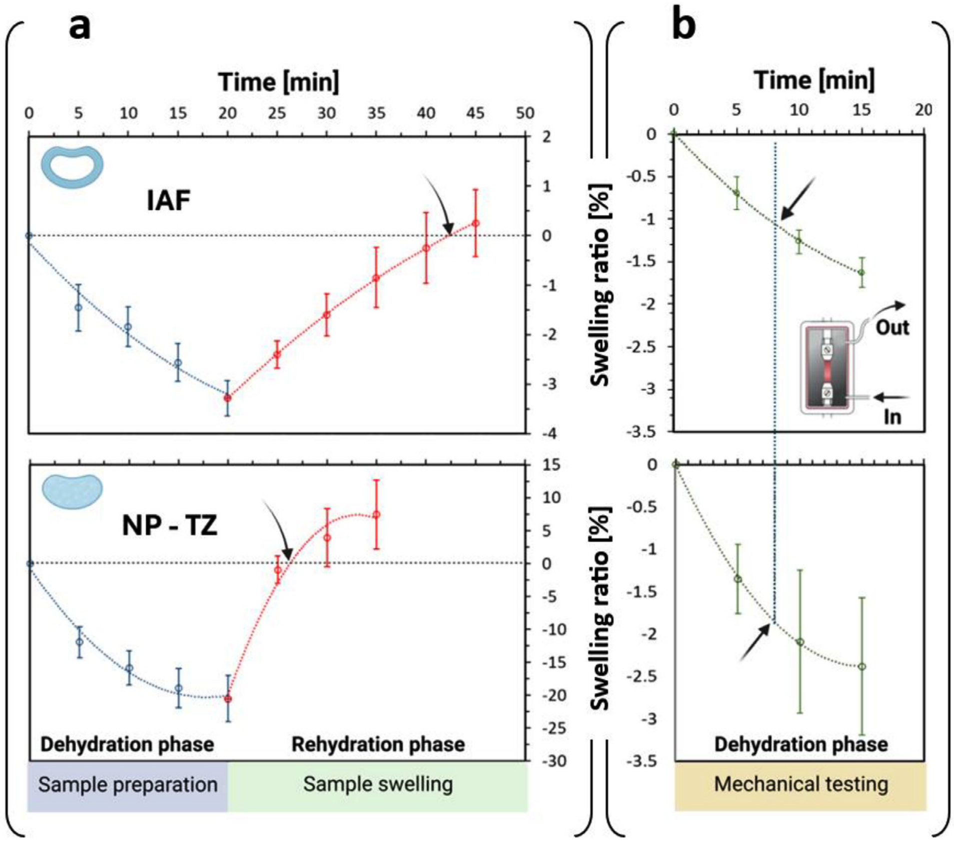

Fig. 2. Swelling (hydration – dehydration) process during sample preparation (a) and water loss during mechanical testing (b). The first dehydration phase (blue lines) indicates tissue water loss during sample preparation. The rehydration phase (red lines) shows the swelling process of tissue in a water bath to identify the required swelling time essential to reach the initial level of tissue hydration as before sample preparation. The curved black arrows in (Fig. 2a) indicate the duration of swelling in a water bath to reach the initial level of tissue hydration. AF, TZ, and NP refer to the annulus fibrosus, transition zone, and nucleus pulposus of the IVD, respectively. The second dehydration phase (green lines in Fig. 2b) indicates tissue water loss in the humidity chamber for more than 500 s. The straight arrows (b) show samples water loss in the humidity chamber at 500 s (duration of mechanical testing). In and out represent water vapour inlet and outlet for the connection of the humidity chamber to a nebulizer.

higher than the NP ($p = 0.001$). The mean (± 95 % CI) equilibrium stresses for the IAF, TZ, and NP were 121.4 ± 20.8, 14.6 ± 6.7, and 4.5 ± 2.4 kPa, respectively. Our statistical analysis revealed that the equilibrium stress was significantly higher for the IAF compared to the TZ and NP ($p < 0.001$) but not between the TZ and NP regions ($p = 0.7$) (Fig. 4d).

The average R^2 values exceeded 0.98 (Table 1), indicating an excellent fit between the model and the data, thereby demonstrating the model's high accuracy in representing the underlying trends within the experimental dataset. Using the Peleg model (Eqs. (2) and (3)), the level of decayed stress (parameter a), rate at which stress is relaxed (parameter b), and the time necessary for stresses to reach 50% of the decayed stress (t_{50}) were calculated (Table 1). Based on Eq. (2), 1/b is the time required to reach the level of stress a/2.

Our statistical analysis revealed that the overall effect of region on both the level of decayed stress (parameter a) and the rate at which stress is relaxed (parameter b) was significant ($p < 0.006$). No significant differences were found for the level of decayed stress ($p = 0.73$) and the rate at which stress is relaxed ($p = 0.23$) for the TZ region at different strain magnitudes (Fig. 5).

Posthoc analysis revealed that the level of decayed stress was significantly lower for the IAF compared to the TZ ($p = 0.001$) and NP ($p = 0.002$) regions (Fig. 5a). Moreover, it was found that the rate at which stress is relaxed was significantly lower ($p = 0.007$) for the IAF compared to the NP (Fig. 5b). Interestingly, the rate at which stress is relaxed in the IAF was not significantly lower than the TZ ($p = 0.8$). It was also revealed that the rate at which TZ stress is relaxed was lower than the NP region ($p = 0.04$). No significant differences were found for the level of decayed stress

Table 1
The mean (± 95 % CI) values for the level of decayed stress (parameter a), the rate at which stress is relaxed (parameter b), the time necessary for stress to reach 50 % of the decayed stress, and the average value for the coefficient of determination (R^2), for different regions and at different TZ initial strains.

	a	b (1/s)	t_{50} (s)	Average R^2
IVD regions [strain = 0.6 mm/mm]				
IAF	0.7 (± 0.03)	0.7 (± 0.03)	12.8 (± 1.8)	0.99 (± 0.001)
TZ	0.9 (± 0.04)	0.14 (± 0.05)	7.7 (± 2.2)	0.99 (± 0.004)
NP	0.9 (± 0.05)	0.3 (± 0.15)	4.0 (± 2.3)	0.98 (± 0.007)
Strains [TZ region]				
0.2 mm/mm	0.8 (± 0.03)	0.10 (± 0.02)	10.5 (± 2.4)	0.98 (± 0.005)
0.4 mm/mm	0.9 (± 0.02)	0.1 (± 0.05)	8.1 (± 1.9)	0.99 (± 0.008)
0.6 mm/mm	0. 9 (± 0.04)	0.14 (± 0.01)	7.7 (± 2.2)	0.99 (± 0.004)

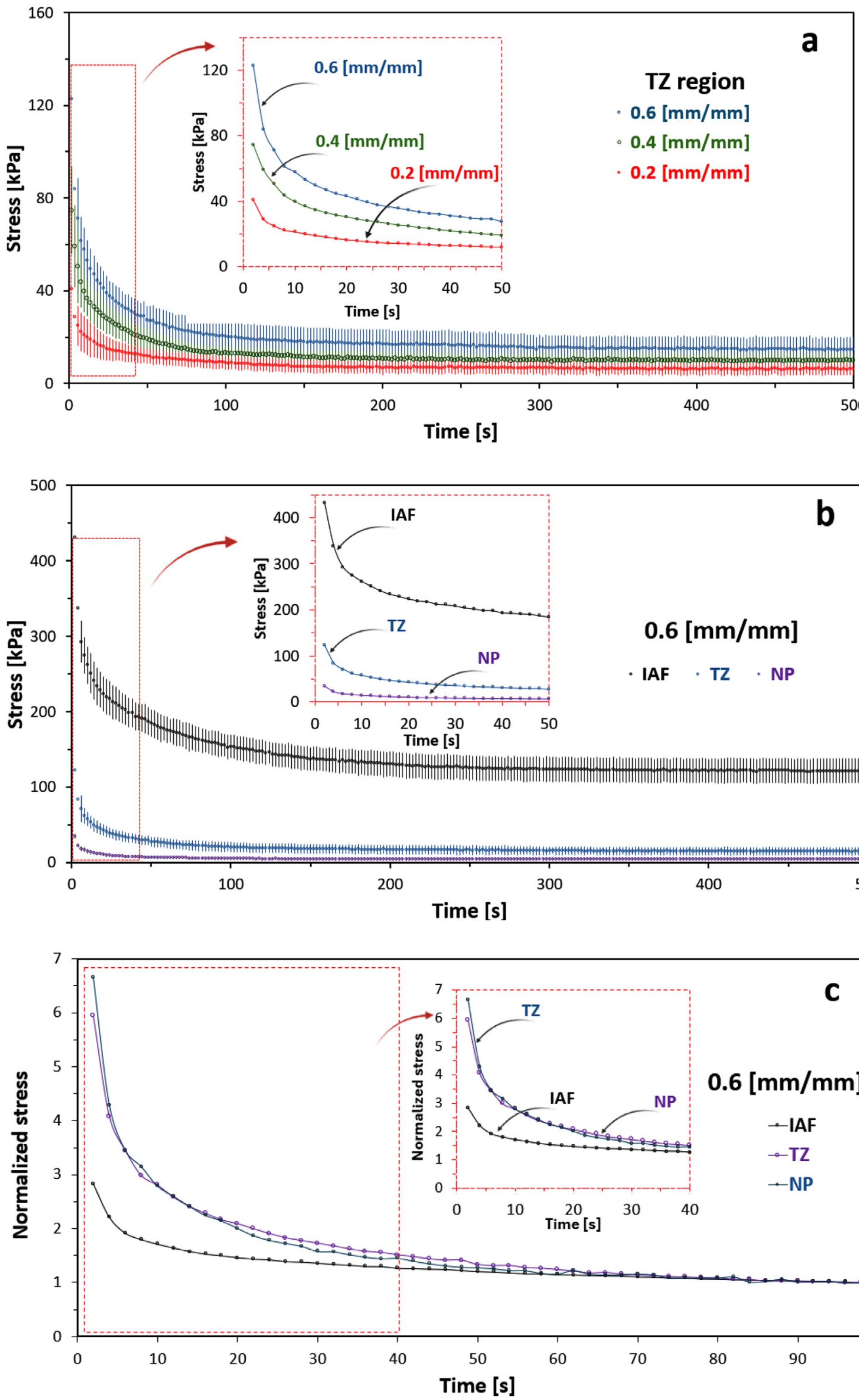

Fig. 3. Stress relaxation data for a) stress relaxation curves (mean ± 95 %CI) for TZ region at different strain magnitudes of 0.2, 0.4, and 0.6 mm/mm including a magnified working range of initial 50 sec (inset), b) stress relaxation curves (mean ± 95 %CI) for different IVD regions (IAF, TZ, and NP) under 0.6 mm/mm strain magnitude including a magnified working range of initial 50 s (inset) and c) stress relaxation curves (mean) using normalized stress (to the equilibrium stress) for different regions of interest (IAF, TZ, and NP) under 0.6 mm/mm strain magnitude including a magnified working range of initial 40 s (inset).

($p = 0.7$) and the rate at which stress is relaxed ($p = 0.231$) at different strain magnitudes for the TZ region (Fig. 5c and d).

For the TZ region, the overall effect of strain magnitudes on t_{50} was not significant ($p = 0.13$). A significant difference was found for t_{50} between different IVD regions ($p < 0.001$). Our posthoc evaluation revealed a significantly higher t50 for the IAF compared to the TZ ($p = 0.007$) and NP ($p < 0.001$). Additionally, t50 was marginally higher for the TZ compared to the NP region ($p = 0.05$) (Fig. 6).

4. Discussion

The current research study aimed to provide new insights into the stress relaxation properties of the TZ compared to the adja-

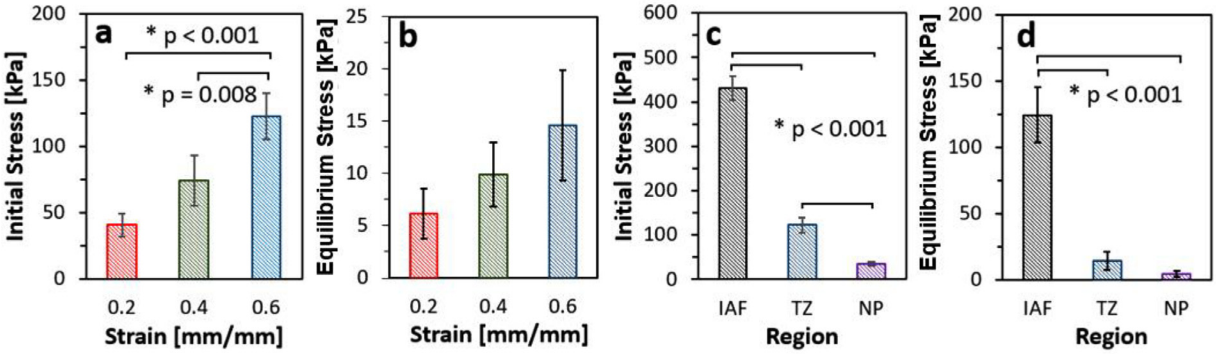

Fig. 4. Stress relaxation data for changes in initial (a) and equilibrium (b) stresses for the TZ region under different strain magnitudes of 0.2, 0.4, and 0.6 mm/mm, as well as changes in initial (c) and equilibrium (d) stresses for different regions of interest (IAF, TZ, and NP) under a strain magnitude of 0.6 mm/mm.

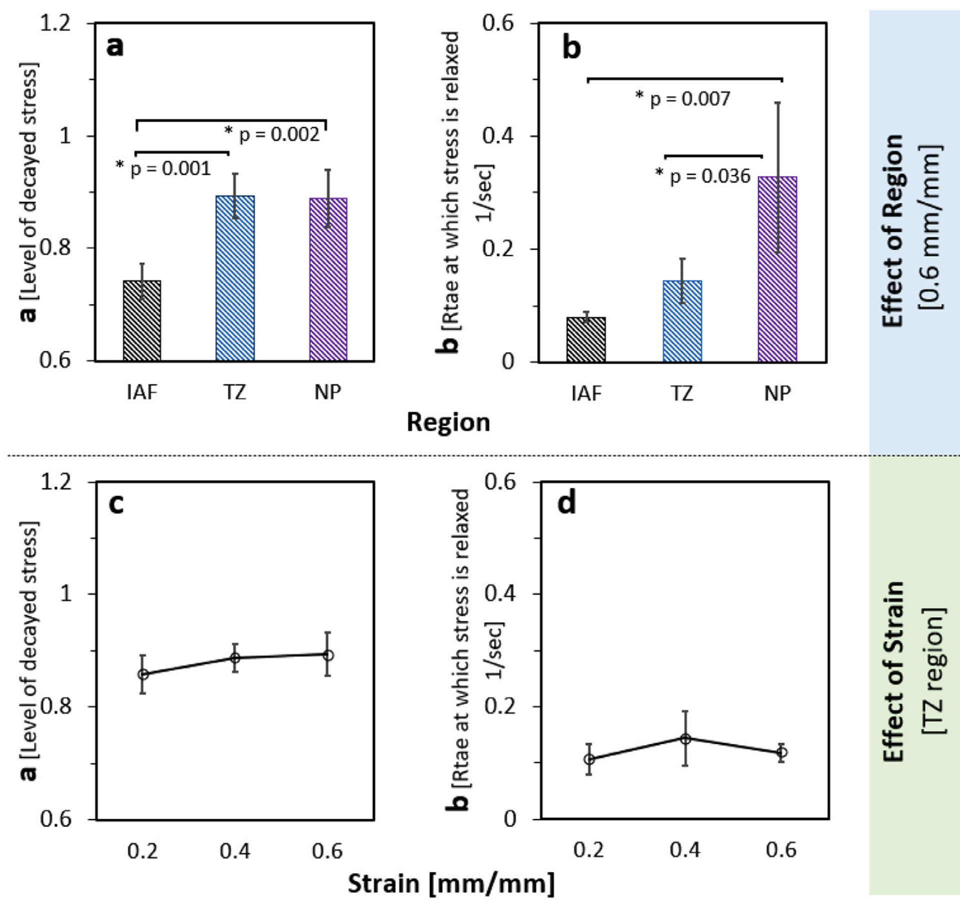

Fig. 5. Outcomes of the Peleg model for stress relaxation analysis indicating the overall effect of the region (a and b) and strain magnitude (0.2, 0.4, and 0.6 mm/mm) on the level and rate of decayed stress (c and d).

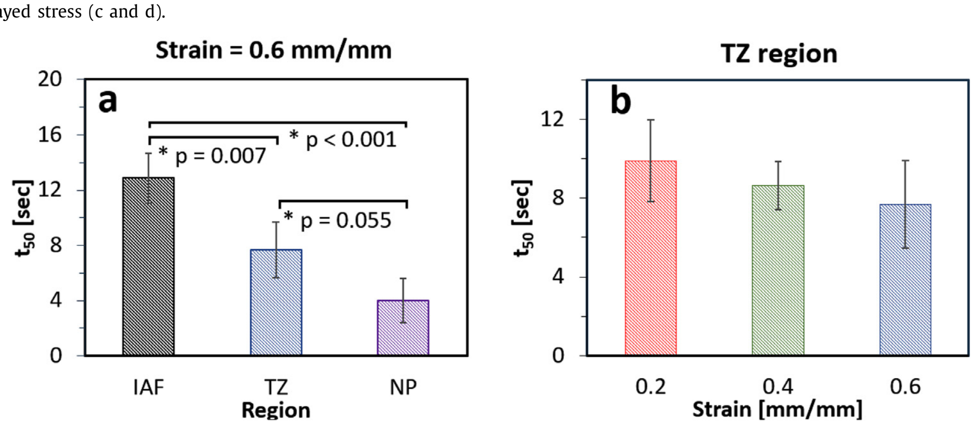

Fig. 6. The effect of (a) region and (b) strain magnitude on t50 (the time necessary for stresses to reach 50 % of the decayed stress).

cent regions of the intervertebral disc (the IAF and NP) in the radial direction, determine their mechanical continuity under stress relaxation conditions, and model their stress relaxation behavior. Prior to the current study, the stress relaxation characteristics of the TZ region were unknown, and how stress is relaxed in the TZ compared to the adjacent IVD regions (NP and IAF) was not fully understood. In the current study, samples from the TZ region were carefully selected and prepared. Understanding the stress relaxation behavior of the TZ region will pave the way for the development of enhanced computational models and biomimetic grafts that present more realistic IVD features, including how the NP and IAF are mechanically related. In addition, the results of the current study may be helpful in creating new technologies, such as organ-on-a-chip models that represent IVD regions with different mechanical, structural and biological characteristics [36].

Sample preparation in the current study was performed based on well-established methodology published in our previous studies [9,10]. The preparation of samples for mechanical testing from the NP and IAF was straightforward, and our approach to selecting the last layer of the IAF as a reference and collecting samples with 3 and 10 mm distance from that (Fig. 1a), to prepare IAF and NP samples respectively, provided consistency and a reproducible method for sample preparation. However, the preparation of TZ samples was challenging due to the size of the region. In our previously published studies, we observed a different structural organization, compared to the rest of the NP, for the elastic and collagen fibers within a 5 mm distance from the last layer of the IAF (toward the NP), which represented the start of the TZ [9,11,31]. Therefore, selecting tissue with a 1 mm length from the last layer of the IAF ensured that the TZ region was selected and that the effect of the IAF lamellae and NP on sample preparation was minimal. It is important to note that we assumed that both TZ and NP regions share approximately similar swelling characteristics which may impose some limitations. This was due to the small size of the TZ region, which made the accurate gravimetric measurement of swelling almost impossible. This approach can be considered as one of the limitations of the current study. The results of the current study showed no significant changes in the swelling ratio between neighbouring time intervals for both the AF and NP-TZ regions ($p < 0.8$), supporting the suitability of the developed technique for characterizing tissue rehydration. However, it is important to consider that the precision of the technique may vary depending on the size, species, and regions of interest.

As expected, we observed different swelling properties for different IVD regions (IAF and NP-TZ), which was predicted to be related to the concentration gradient of IVD glycoproteins and the type of collagen fibers from the NP towards the AF, as well as microstructural changes between the regions [37–41]. The current study introduced a swelling (pre-conditioning) protocol for the measurement of micromechanical properties using ovine IVDs and revealed that the use of a humidity chamber could reduce IVD water loss to less than 2 % for a long stress relaxation (Fig. 2).

The first aim of the current study was to understand the effect of strain magnitude on the stress relaxation properties of the TZ region. We observed a similar trend for the TZ stress decay under different strain magnitudes of 0.2, 0.4, and 0.6 mm/mm, with no significant differences observed for t50 between different strain magnitudes (Fig. 6b). However, we found significantly higher initial stress for the 0.6 mm/mm strain compared to the 0.4 mm/mm (40 %; $p = 0.008$) and 0.2 mm/mm (67 %; $p < 0.001$) strain magnitudes (Fig. 4a). The TZ initial stress for the 0.4 mm/mm strain was higher (marginally significant, $p = 0.06$) than that of for 0.2 mm/mm strain magnitude. Additionally, we observed that for all strain magnitudes, the final average TZ stress was not decayed to zero; however, the difference between equilibrium stresses was marginally significant (Fig. 4b; $p = 0.05$). The observation of marginally significant differences in equilibrium and initial stresses between different strain magnitudes may be relevant to the sample size, which can be considered another limitation of the current study. Our previous studies to measure and characterize the microstructural and micromechanical properties of the AF lamellae, interlamellar matrix (ILM), NP and TZ have recruited 6 to 10 samples where the observed powers were > 0.9 [10,11,34,42,43]. In the current study, we employed 6 samples in each group sample (30 samples in total) to identify the stress relaxation parameters, which seems adequate to ensure true differences are found. It is important to note that our previous study on the mechanical characterization of TZ region revealed that strain magnitudes below 70% were unlikely to create permanent defects in the TZ microstructure [9]. The TZ region exhibited a nonlinear viscoelastic behavior with an average strain of 69% (± 8.8 %) at maximum stress. This might explain why the impact of strain magnitudes (0.2, 0.4, and 0.6 mm/mm) on relaxation parameters was not significant (Fig. 5c and b). In the current research, the ramp time was less than 0.4 seconds. Whether this duration was sufficient to minimize tissue relaxation during initial loading is unclear. This should be considered as another limitation of the study. Another limitation of this study was the use of an ovine model. Despite significant evidence supporting ovine models for their structural and biochemical resemblance to human IVDs the use of human samples would offer more clinically relevant insights [44,45].

The second aim of the study was to identify how stress is relaxed in the TZ compared to the adjacent regions of the IVD (IAF and NP) under 0.6 mm/mm strain magnitude. Our previously published studies found that structural failure of the AF tissue in the IVD initiates at 60–70 % radial stretch and delamination of the AF layers may occur. Therefore, in this study, we chose 0.6 mm/mm stretch to compare how stress is relaxed in the TZ (compared to the AF and NP regions) when the risk of failure in the AF is high [33,34]. Our experimental stress relaxation data revealed a significantly higher equilibrium stress for the IAF compared to the TZ and NP regions ($p < 0.001$) but not between the TZ and IAF regions ($p = 0.7$). We found that NP radial stress was relaxed significantly faster ($p < 0.04$) compared to the TZ and NP (Fig. 5b); however, this rate was not significantly different between the IAF and TZ. The initial stress was significantly higher for the IAF (431.4 ± 27.8 kPa) compared to the TZ (> 3 times; $p < 0.001$) and NP (> 12 times; $p < 0.001$) regions. In addition, the initial TZ stress was significantly higher compared to that of the NP (> 3.7 times; $p = 0.001$) (Fig. 4c). We found a significantly higher t50 for the IAF compared to the TZ ($p = 0.007$) and NP ($p < 0.001$). Additionally, t50 was marginally higher for the TZ compared to the NP region ($p = 0.05$) (Fig. 6).

In the current research, we employed the mathematical model proposed by Peleg to identify the stress relaxation behavior of different IVD regions. The Peleg mathematical equation presents a simple model with only two constants (level of decayed stress and rate of stress relaxation). The outcomes of the model were consistent with experimental data indicating that the overall effect of region on both the level of decayed stress (parameter a) and the rate at which stress is relaxed (parameter b) was significant ($p < 0.01$). The IAF exhibited significantly lower decayed stress compared to the TZ ($p = 0.001$) and NP ($p = 0.002$) regions (Fig. 5a). The result of the current study revealed that the stress relaxation rate and decayed stress exhibited an increasing trend from the IAF towards the NP, which were in the opposite trend to the hysteresis area and modulus [9]. The Peleg model was used in this study due to its simplicity, akin to the quasi-linear viscoelastic model, which facilitates the comparison of relaxation parameters across different regions of interest at various strain rates and magnitudes. This model allows for the straightforward calculation of stress relaxation parameters at a single strain level. However, it is important to note

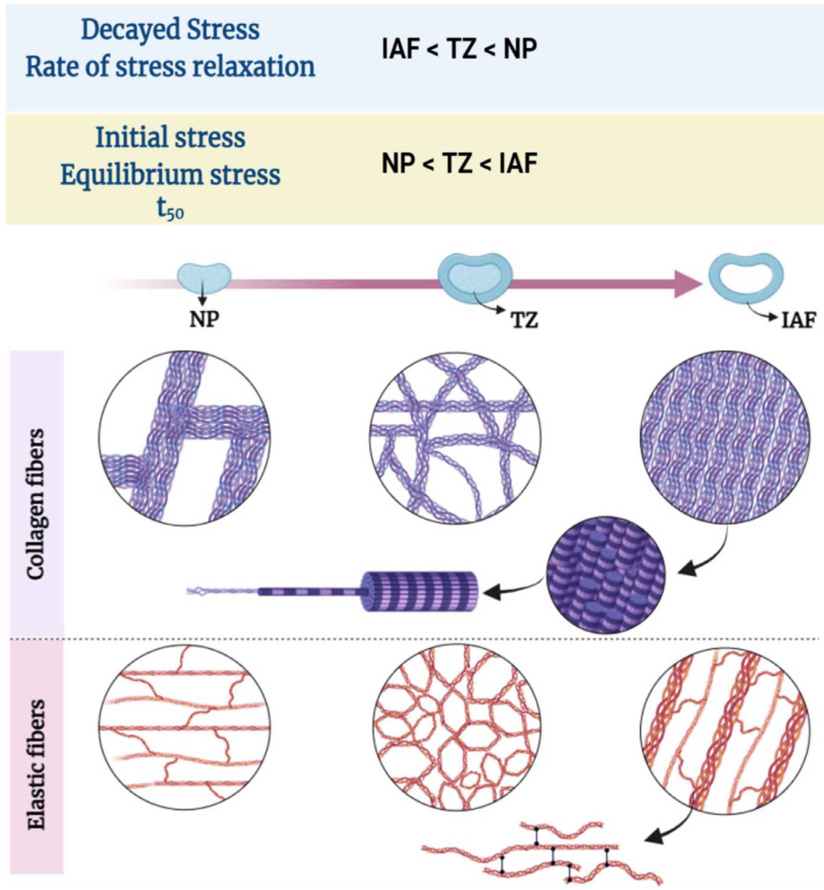

Fig. 7. Schematic of the microstructural organization of collagen and elastic fibers within the NP, TZ and IAF regions, including changes in stress relaxation parameters (under 0.6 mm/mm strain) from the NP towards the IAF. The length scale microstructural organization of fibers indicates that like collagen, elastic fibers are composed of cross-linked microfibrils but with different lengths.

that constitutive law might offer improved predictive accuracy by capturing nonlinearities in the stress relaxation responses [46].

The current study investigated how stress is relaxed between adjacent regions of the IVD (IAF, TZ, and NP) in the radial direction. The focus of this research was to identify the stress relaxation properties of the TZ, compared to the adjacent regions, and therefore, the associated mechanism was not directly explored. However, shape transformation is likely to explain different relaxation properties between different IVD regions. Different studies have shown that bilayered hydrogels with varying viscoelastic properties often exhibit mismatched recovery rates after being released from a pre-stretched state, resulting in shape transformation [47–49]. This phenomenon is linked to the kinetics of physical associations and the entropic elasticity of molecular chains, which cause a temporary configuration before full recovery to the original shape [49]. It's important to recognize that shape transformation can also occur due to swelling mismatches in bilayer hydrogels or those with a gradient microstructure [50–52]. These materials have different stiffness and diffusion properties, leading to varying volume changes causing shape changes. Additionally, a similar viscoelastic mismatch is often observed in nature; for example, the leaves of the Mimosa pudica plant quickly curl up and then gradually recover after being touched [53]. This process involves spontaneous shape-shifting to form three-dimensional structures, followed by self-recovery to the original form. In the current study, we found (normalized stress relaxation data, Fig. 3c) similar stress relaxation characteristics between the NP and TZ regions. However, the IAF exhibited a mismatch in stress relaxation characteristics compared to the NP and TZ. It is possible that this mismatch in stress relaxation acts as a shape transformation mechanism triggered by viscoelastic behavior, as shown for synthetic materials [49]. Our previous study revealed that changes in the IVD structure and composition of the IAF-TZ-NP tissue block induced gradient hyperelastic behavior [9]. In this study, we observed both swelling and relaxation mismatches between the NP and TZ when compared to the IAF.

Stress relaxation is mainly attributed to the sliding of collagen fibers and fibrils as well as their interactions with other components of the extracellular matrix such as PGs and GAGs [54–57]. In addition, shape transformation can be explained based on the differences in microstructural organization between the IVD regions. In our previously published studies, we found that the NP collagen fibers were mostly orientated toward the top and bottom vertebrae, while elastic fibers were more radially orientated toward the AF. In contrast, both elastic and collagen fibers were highly radially orientated within the TZ region, creating a honeycomb microstructure that was mechanically connected to the fibers in the IAF region. Highly interconnected fibers (both collagen and elastic fibers) in the IAF created a substantially compact and dense network that controlls the viscoelastic properties of the region. Both collagen and elastic fibers in the NP and TZ regions, which are physically and mechanically integrated, create a looser fiber network compared to the TZ regions, leading to a steeper descent of the relaxation curve toward the equilibrium values (Fig. 7). This also explains the significant effect of IVD regions on t_{50} (the time necessary for stresses to reach 50 % of the decayed stress) indicating a decreasing trend from the IAF towards the NP. Different studies have shown the impact of collagen fibers, PGs, and

GAGs in the viscoelastic behavior of soft tissues, indicating that elastic fibers may contribute less to the viscoelastic characteristics [54–57]. This conclusion has been made based on the observation of the positive correlation between collagen content and changes in relaxation modes and trends. Therefore, collagen fibres are perhaps the most important fibrous component contributing to the time-dependent behaviour of the soft tissues. However, our previously published studies revealed that the interlamellar matrix of the AF in IVD, with a high concentration of elastic fibers, exhibited viscoelastic properties [34]. This suggests that while non-elastic components of the IVD play a significant role in its viscoelastic behavior, the role of elastic fibers should not be ignored. In fact, mechanically integrated fiber structures or designs (composed of both collagen and elastin) with different multiscale structural organizations which are assembled in a high water-content PG and GAG matrix, may control the viscoelastic characteristics of IVD. It is highly likely that elastic behavior in small strains of the IAF-TZ-NP tissue is mainly controlled by the elastic fiber network, while other components of the extracellular matrix (including PGs, GAGs, and collagen) govern the large deformations, hyperelastic and viscoelastic behavior. From a structural point of view, the size, orientation, density, and shape factor of elastic fibers are significantly different between various IVD regions including the IAF, TZ, and NP which may contribute to the viscoelastic and stress relaxation properties of the IVD [58–60]. The introduction of “shape transformation” as a plausible mechanism for changes in decayed stress from the NP towards the IAF may be clinically relevant. However, it requires further investigation to understand whether the proposed mechanism can induce tissue failure during radial extension.

5. Conclusion

This study, for the first time, identified the stress relaxation properties of the transition zone (TZ) in the IVD under different magnitudes and revealed how stress relaxation parameters are altered from the NP towards the IAF. For the TZ region, the initial tissue stress was higher for higher strain magnitudes with an increasing trend from 0.2 to 0.6 mm/mm; however, t_{50} (the time necessary for stresses to reach 50 % of the decayed stress) was not significantly different. We found that the overall effect of region on initial stress, equilibrium stress, level of decayed stress, the rate at which stress is relaxed, and t_{50} was significant. The results of the current study revealed a mismatch for stress relaxation properties, based on normalized data of the different regions. This proposed “tissue shape transformation” as a mechanism for stress relaxation changes between IVD regions and, more specifically, between the IAF and TZ. Changes in microstructural organization of collagen and elastic fibers and variation in composition and concentration of the IVD extracellular matrix components, as well as biochemical links and mechanical entanglement within the fibrous structure can potentially justify the significant effect of regions and strain magnitudes on the stress relaxation behavior of IVD.

Declaration of competing interest

The authors declare that they have no known competing financial interests or personal relationships that could have appeared to influence the work reported in this paper.

CRediT authorship contribution statement

Lydia Vieira: Writing – original draft, Project administration, Methodology, Investigation, Formal analysis. **Haim S Mordechai:** Writing – original draft, Formal analysis, Data curation. **Mirit Sharabi:** Writing – review & editing, Validation, Supervision, Formal analysis, Data curation, Conceptualization. **Joanne L. Tipper:** Writing – review & editing, Validation, Supervision, Resources, Conceptualization. **Javad Tavakoli:** Writing – review & editing, Visualization, Supervision, Project administration, Formal analysis, Data curation, Conceptualization.

References

[1] J. Cassidy, A. Hiltner, E. Baer, Hierarchical structure of the intervertebral disc, Connect. Tissue Res. 23 (1) (1989) 75–88.
[2] M. Humzah, R. Soames, Human intervertebral disc: structure and function, Anatom. Record 220 (4) (1988) 337–356.
[3] K.-W. Kim, T.-H. Lim, J.G. Kim, S.-T. Jeong, K. Masuda, H.S. An, The origin of chondrocytes in the nucleus pulposus and histologic findings associated with the transition of a notochordal nucleus pulposus to a fibrocartilaginous nucleus pulposus in intact rabbit intervertebral discs, Spine 28 (10) (2003) 982–990.
[4] D. Cyril, A. Giugni, S.S. Bangar, M. Mirzaeipoueinak, D. Shrivastav, M. Sharabi, J.L. Tipper, J. Tavakoli, Elastic fibers in the intervertebral disc: from form to function and toward regeneration, Int. J. Mol. Sci. 23 (16) (2022) 8931.
[5] P. Ghosh, T. Taylor, B. Horsburgh, The composition and protein metabolism in the immature rabbit intervertebral disc, Cell Tissue Res. 163 (1975) 223–238.
[6] W.A. Souter, T.K. Taylor, Sulphated acid mucopolysaccharide metabolism in the rabbit intervertebral disc, J. Bone Joint Surg. Bri. 52 (2) (1970) 371–384.
[7] F. Guilak, H.P. Ting-Beall, A.E. Baer, W.R. Trickey, G.R. Erickson, L.A. Setton, Viscoelastic properties of intervertebral disc cells: identification of two biomechanically distinct cell populations, Spine 24 (23) (1999) 2475.
[8] H.-J. Hansen, S. Ullberg, Uptake of S35 in the intervertebral discs after injection of S35-sulphate. An autoradiographic study, Acta Orthopaed. Scand. 30 (1-4) (1961) 84–90.
[9] M. Mirzaeipoueinak, H.S. Mordechai, S.S. Bangar, M. Sharabi, J.L. Tipper, J. Tavakoli, Structure-function characterization of the transition zone in the intervertebral disc, Acta Biomater. 160 (2023) 164–175.
[10] J. Tavakoli, J.L. Tipper, Detailed mechanical characterization of the transition zone: New insight into the integration between the annulus and nucleus of the intervertebral disc, Acta Biomater. 143 (2022) 87–99.
[11] J. Tavakoli, A.D. Diwan, J.L. Tipper, The ultrastructural organization of elastic fibers at the interface of the nucleus and annulus of the intervertebral disk, Acta Biomater. 114 (2020) 323–332.
[12] H. Yao, W.Y. Gu, Physical signals and solute transport in human intervertebral disc during compressive stress relaxation: 3D finite element analysis, Biorheology 43 (3-4) (2006) 323–335.
[13] J.C. Iatridis, M. Weidenbaum, L.A. Setton, V.C. Mow, Is the nucleus pulposus a solid or a fluid? Mechanical behaviors of the nucleus pulposus of the human intervertebral disc, Spine 21 (10) (1996) 1174–1184.
[14] S.E. Bezci, S. Lim, G.D. O'Connell, Nonlinear stress-dependent recovery behavior of the intervertebral disc, J. Mech. Behav. Biomed. Mater. 110 (2020) 103881.
[15] Y.-W. Kuo, J.-L. Wang, Rheology of intervertebral disc: an: ex vivo: study on the effect of loading history, loading magnitude, fatigue loading, and disc degeneration, Spine 35 (16) (2010) E743–E752.
[16] G.D. O'Connell, E.J. Vresilovic, D.M. Elliott, Human intervertebral disc internal strain in compression: the effect of disc region, loading position, and degeneration, J. Orthop. Res. 29 (4) (2011) 547–555.
[17] N.D. Panagiotacopulos, M.H. Pope, M.H. Krag, R. Bloch, A mechanical model for the human intervertebral disc, J. Biomech. 20 (9) (1987) 839–850.
[18] A.M. Ellingson, D.J. Nuckley, Intervertebral disc viscoelastic parameters and residual mechanics spatially quantified using a hybrid confined/in situ indentation method, J. Biomech. 45 (3) (2012) 491–496.
[19] A.J. van der Veen, A. Bisschop, M.G. Mullender, J.H. van Dieën, Modelling creep behaviour of the human intervertebral disc, J. Biomech. 46 (12) (2013) 2101–2103.
[20] K. Kandil, F. Zaïri, A. Derrouiche, T. Messager, F. Zaïri, Interlamellar-induced time-dependent response of intervertebral disc annulus: a microstructure-based chemo-viscoelastic model, Acta Biomater. 100 (2019) 75–91.
[21] S.R. Lucas, C.R. Bass, R.S. Salzar, M.L. Oyen, C. Planchak, A. Ziemba, B.S. Shender, G. Paskoff, Viscoelastic properties of the cervical spinal ligaments under fast strain-rate deformations, Acta Biomater. 4 (1) (2008) 117–125.
[22] R.N. Natarajan, J.R. Williams, G.B.J. Andersson, Modeling changes in intervertebral disc mechanics with degeneration, JBJS 88 (suppl_2) (2006) 36–40.
[23] S.E. Bezci, G.D. O'Connell, Osmotic pressure alters time-dependent recovery behavior of the intervertebral disc, Spine 43 (6) (2018) E334–E340.
[24] W. Johannessen, E.J. Vresilovic, A.C. Wright, D.M. Elliott, Intervertebral disc mechanics are restored following cyclic loading and unloaded recovery, Ann. Biomed. Eng. 32 (2004) 70–76.
[25] P. Swider, A. Pédrono, D. Ambard, F. Accadbled, J. Sales de Gauzy, Substructuring and poroelastic modelling of the intervertebral disc, J. Biomech. 43 (7) (2010) 1287–1291.
[26] K.M. Groth, K.P. Granata, The viscoelastic standard nonlinear solid model: predicting the response of the lumbar intervertebral disk to low-frequency vibrations, J. Biomech. Eng. 130 (3) (2008).
[27] N. Yoganandan, S. Umale, B. Stemper, B. Snyder, Fatigue responses of the human cervical spine intervertebral discs, J. Mech. Behav. Biomed. Mater. 69 (2017) 30–38.
[28] H.R. Newman, J.F. DeLucca, J.M. Peloquin, E.J. Vresilovic, D.M. Elliott, Multiaxial validation of a finite element model of the intervertebral disc with multigenerational fibers to establish residual strain, JOR SPINE 4 (2) (2021) e1145.

[29] K. Fujii, A. Lai, N. Korda, W.W. Hom, T.W. Evashwick-Rogler, P. Nasser, A.C. Hecht, J.C. Iatridis, Ex-vivo biomechanics of repaired rat intervertebral discs using genipin crosslinked fibrin adhesive hydrogel, J. Biomech. 113 (2020) 110100.
[30] M.A. Chetoui, O. Boiron, M. Ghiss, A. Dogui, V. Deplano, Assessment of intervertebral disc degeneration-related properties using finite element models based on $$\uprho _H$$-weighted MRI data, Biomech. Model. Mechanobiol. 18 (1) (2019) 17–28.
[31] J. Tavakoli, A.D. Diwan, J.L. Tipper, Elastic fibers: The missing key to improve engineering concepts for reconstruction of the Nucleus Pulposus in the intervertebral disc, Acta Biomater. 113 (2020) 407–416.
[32] J. Tavakoli, J.J. Costi, New insights into the viscoelastic and failure mechanical properties of the elastic fiber network of the inter-lamellar matrix in the annulus fibrosus of the disc, Acta Biomater. 77 (2018) 292–300.
[33] J. Tavakoli, D.B. Amin, B.J.C. Freeman, J.J. Costi, The biomechanics of the inter-lamellar matrix and the lamellae during progression to lumbar disc herniation: which is the weakest structure? Ann. Biomed. Eng. 46 (9) (2018) 1280–1291.
[34] J. Tavakoli, J.J. Costi, New findings confirm the viscoelastic behaviour of the inter-lamellar matrix of the disc annulus fibrosus in radial and circumferential directions of loading, Acta Biomater. 71 (2018) 411–419.
[35] M. PELEG, Characterization of the stress relaxation curves of solid foods, J. Food Sci. 44 (1) (1979) 277–281.
[36] J. Tavakoli, A.D. Diwan, J.L. Tipper, Intervertebral disc-on-a-chip: a precision engineered toolbox for low back pain studies, Trends Biotechnol. 41 (11) (2023) 1339–1342.
[37] J. Tavakoli, Region–media coupling in characterization and modelling of the disc annulus single lamella swelling, Med. Biol. Eng. Comput. 55 (8) (2017) 1483–1492.
[38] D.H. Cortes, N.T. Jacobs, J.F. DeLucca, D.M. Elliott, Elastic, permeability and swelling properties of human intervertebral disc tissues: a benchmark for tissue engineering, J. Biomech. 47 (9) (2014) 2088–2094.
[39] S.E. Bezci, K. Torres, C. Carraro, D. Chiavacci, B. Werbner, S. Lim, G.D. O'Connell, Transient swelling behavior of the bovine caudal disc, J. Mech. Behav. Biomed. Mater. 112 (2020) 104089.
[40] J.C. Iatridis, M. Weidenbaum, L.A. Setton, V.C. Mow, Is the nucleus pulposus a solid or a fluid? Mechanical behaviors of the nucleus pulposus of the human intervertebral disc, Spine 21 (10) (1996).
[41] J.C. Iatridis, J.J. MacLean, M. O'Brien, I.A. Stokes, Measurements of proteoglycan and water content distribution in human lumbar intervertebral discs, Spine (Phila Pa 1976) 32 (14) (2007) 1493–1497.
[42] J. Tavakoli, D.M. Elliott, J.J. Costi, The ultra-structural organization of the elastic network in the intra- and inter-lamellar matrix of the intervertebral disc, Acta Biomater. 58 (2017) 269–277.
[43] J. Tavakoli, J.J. Costi, Ultrastructural organization of elastic fibres in the partition boundaries of the annulus fibrosus within the intervertebral disc, Acta Biomater. 68 (2018) 67–77.
[44] H.-J. Wilke, A. Kettler, L.E. Claes, Are sheep spines a valid biomechanical model for human spines? Spine 22 (20) (1997) 2365–2374.
[45] G.D. O'Connell, E.J. Vresilovic, D.M. Elliott, Comparison of animals used in disc research to human lumbar disc geometry, Spine 32 (3) (2007) 328–333.
[46] F.M. Davis, R. De Vita, A nonlinear constitutive model for stress relaxation in ligaments and tendons, Ann. Biomed. Eng. 40 (12) (2012) 2541–2550.
[47] Z. Huang, X. Chen, S.J.K. O'Neill, G. Wu, D.J. Whitaker, J. Li, J.A. McCune, O.A. Scherman, Highly compressible glass-like supramolecular polymer networks, Nat. Mater. 21 (1) (2022) 103–109.
[48] Y.J. Wang, X.N. Zhang, Y. Song, Y. Zhao, L. Chen, F. Su, L. Li, Z.L. Wu, Q. Zheng, Ultrastiff and tough supramolecular hydrogels with a dense and robust hydrogen bond network, Chem. Mater. 31 (4) (2019) 1430–1440.
[49] X.P. Hao, C.W. Zhang, W. Hong, M. Meng, L.X. Hou, M. Du, Q. Zheng, Z.L. Wu, Engineering viscoelastic mismatch for temporal morphing of tough supramolecular hydrogels, Mater. Horiz. 10 (2) (2023) 432–442.
[50] S.J. Jeon, A.W. Hauser, R.C. Hayward, Shape-morphing materials from stimuli-responsive hydrogel hybrids, Acc. Chem. Res. 50 (2) (2017) 161–169.
[51] X.P. Hao, Z. Xu, C.Y. Li, W. Hong, Q. Zheng, Z.L. Wu, Kirigami-design-enabled hydrogel multimorphs with application as a multistate switch, Adv. Mater. 32 (22) (2020) e2000781.
[52] H. Na, Y.-W. Kang, C.S. Park, S. Jung, H.-Y. Kim, J.-Y. Sun, Hydrogel-based strong and fast actuators by electroosmotic turgor pressure, Science 376 (6590) (2022) 301–307.
[53] R.D. Allen, Mechanism of the seismonastic reaction in mimosa pudica, Plant Physiol. 44 (8) (1969) 1101–1107.
[54] H.S. Gupta, J. Seto, S. Krauss, P. Boesecke, H.R.C. Screen, In situ multi-level analysis of viscoelastic deformation mechanisms in tendon collagen, J. Struct. Biol. 169 (2) (2010) 183–191.
[55] H.R.C. Screen, S. Toorani, J.C. Shelton, Microstructural stress relaxation mechanics in functionally different tendons, Med. Eng. Phys. 35 (1) (2013) 96–102.
[56] H.R.C. Screen, J. Seto, S. Krauss, P. Boesecke, H.S. Gupta, Extrafibrillar diffusion and intrafibrillar swelling at the nanoscale are associated with stress relaxation in the soft collagenous matrix tissue of tendons, Soft Matter 7 (23) (2011) 11243–11251.
[57] A. Anssari-Benam, H.R.C. Screen, A. Bucchi, Insights into the micromechanics of stress-relaxation and creep behaviours in the aortic valve, J. Mech. Behav. Biomed. Mater. 93 (2019) 230–245.
[58] F. Burla, Y. Mulla, B.E. Vos, A. Aufderhorst-Roberts, G.H. Koenderink, From mechanical resilience to active material properties in biopolymer networks, Nat. Rev. Phys. 1 (4) (2019) 249–263.
[59] B.A. Kozel, R.P. Mecham, Elastic fiber ultrastructure and assembly, Matrix Biol. 84 (2019) 31–40.
[60] J.-Y. Lin, J.-S. Huang, Stress relaxation of cellular materials, J. Compos. Mater. 39 (3) (2005) 233–245.